frontiers | Frontiers in Earth Science

TYPE Original Research
PUBLISHED 19 January 2023
DOI 10.3389/feart.2022.1042477

OPEN ACCESS

EDITED BY
Zhenzhi Wang,
Henan Polytechnic University, China

REVIEWED BY
Zhang Kun,
Anhui University of Science and Technology, China
Haichao Wang,
Xinjiang University, China

*CORRESPONDENCE
Wei Wang,
wangweiuuu@163.com
Qinghe Niu,
qinghniu@163.com

†PRESENT ADDRESS
Qizhi Wang,
School of Civil Engineering, Hebei University of Science and Technology, Shijiazhuang, China

SPECIALTY SECTION
This article was submitted to Economic Geology,
a section of the journal
Frontiers in Earth Science

RECEIVED 12 September 2022
ACCEPTED 20 October 2022
PUBLISHED 19 January 2023

CITATION
Niu Q, Hu M, Leng B, He X, Su W, Wang W, Wang Q, Chang J, Ji Z and Qi X (2023), Experimental and numerical model of anisotropic permeability and CO_2 injectivity of coal during CO_2 enhanced coalbed methane recovery process.
Front. Earth Sci. 10:1042477.
doi: 10.3389/feart.2022.1042477

Experimental and numerical model of anisotropic permeability and CO_2 injectivity of coal during CO_2 enhanced coalbed methane recovery process

Qinghe Niu[1,2,3]*, Mingwei Hu[1,2,3], Bing Leng[4], Xiang He[5], Wenjie Su[6], Wei Wang[1,2,3]*, Qizhi Wang[7†], Jiangfang Chang[1,2], Zhongmin Ji[8] and Xiaofei Qi[9]

[1]State Key Laboratory of Mechanical Behavior and System Safety of Traffic Engineering Structures, Shijiazhuang Tiedao University, Shijiazhuang, China, [2]Hebei Technology and Innovation Center on Safe and Efficient Mining of Metal Mines, Shijiazhuang, China, [3]Key Laboratory of Roads and Railway Engineering Safety Control (Shijiazhuang Tiedao University), Ministry of Education, Shijiazhuang, China, [4]The Second Drilling Engineering Branch of CNPC Bohai Drilling Engineering Co., Ltd., PetroChina, Renqiu, China, [5]Institute of Geology, The Fourth Oil Production Plant of Changqing Oilfield Company, PetroChina Company Limited., Jingbian, China, [6]Exploration Division of Changqing Oilfield Company, PetroChina Company Limited., Xi'an, China, [7]Innovation Center of Disaster Prevention and Mitigation Technology for Geotechnical and Structural Systems of Hebei Province (Preparation), Shijiazhuang, China, [8]School of Civil Engineering, Zhengzhou University of Technology, Zhengzhou, China, [9]The Second Geological Team of Hebei Coalfield Geology Bureau, Xingtai, China

Guaranteeing CO_2 injectivity has been the precondition for implementing the CO_2-enhanced coalbed methane recovery (CO_2-ECBM), however, it dramatically decreases during the CO_2 injection process because it is influenced by the dynamic change of the anisotropic permeability of coal. To reveal and evaluate the CO_2 injectivity of coal, the anisotropic permeability test and the CO_2 injectivity simulation test were first conducted, then the corresponding numerical models were established and verified by the experimental data. The results show that the permeability of coal in parallel face cleat direction is the largest, followed by the permeability of coal in parallel butt cleat direction and that in vertical bedding direction is the minimum. The peak value of the instantaneous injectivity rate is enhanced and the injection time is prolonged with the increase of the CO_2 injection pressure. The total CO_2 injectivity rate is nonlinearly increased from 13.61 to 311.87 cm^2/MPa min when the CO_2 injection pressure raises from 2 to 10 MPa. The anisotropic permeability model is appropriate to describe the dynamic evolution of permeability under different boundary conditions, the CO_2 injectivity prediction model can be used to evaluate the CO_2 injectivity during the CO_2 injection process. Increasing the CO_2 injection pressure may temporarily promote CO_2 injectivity, while the CO_2 injection increment is limited. The CO_2 fracturing by phase transition may be an available reservoir stimulation method for enhancing the CO_2 injection and should be focused on in the future.

KEYWORDS
CO_2-ECBM, adsorption swelling, injection pressure, cleat, CO_2 injectivity

Introduction

In 2018, China's total coal consumption has reached 2.74 billion tons. Although the Chinese government is adjusting its energy structure, it is predicted that the coal consumption demand is up to 50% of total energy consumption in 2025 (Xie et al., 2019). Coal burning has caused a lot of additional environmental problems, such as the sharp increase in greenhouse gas emissions and some heavily polluted weather (Rao and Rubin, 2002; Liu et al., 2021). The Chinese government pledges to reach a peak in its emissions by 2030 and strives to achieve carbon neutrality by 2,060, and a set of carbon emission reduction actions have been established. The carbon capture, utilization, and storage (CCUS) technology have been identified as the only option for substantially reducing GHG emission intensities while using fossil-fuel-based processes (Xu et al., 2019; Janzen et al., 2020). According to the differences in the geological reservoirs, the main CCUS forms are: utilizing CO_2 for enhanced oil recovery (CO_2-EOR) (Wei et al., 2019), gas recovery (CO_2-EGR) (Shi et al., 2017), coalbed methane (CO_2-ECBM) (Niu et al., 2017a; Niu et al., 2020a). As clean and efficient energy, the exploration and development of coalbed methane (CBM) can both relieve the energy crisis and improve the safety of coal mine operations (Wen et al., 2020; Niu et al., 2022). The Chinese government and related enterprises have advocated some technologies to improve the CBM extraction rate, among them, CO_2-ECBM is an effective and significant feasible way, and lots of pilot tests have been implemented all over the world (Godec et al., 2014; Pan et al., 2018). The theoretical basis of CO_2-ECBM is that the adsorption capacity of CO_2 on coal is stronger than that of CH_4, more CH_4 molecules are replaced and displaced out of the coal seam with the benefit of their competitive adsorption effect. However, the volumetric swelling induced by CO_2 adsorption is extremely serious, which compresses the space of fractures in coal seam and causes the significant attenuation of the reservoir permeability (Wang et al., 2020; Wang et al., 2021) and the CO_2 injectivity (Kumar et al., 2012), which has been confirmed by field tests (van Bergen et al., 2006; Shi et al., 2008). Guaranteeing CO_2 injectivity has been the precondition for implementing the CO_2-enhanced coalbed methane recovery (CO_2-ECBM) (Niu et al., 2021a).

For this issue, many researchers analyzed the evolution mechanism of coal permeability during the CO_2 injection process. Lin et al. found that the permeability reduction can reach 13 %–70% for the CO_2 exposure time in different testings (Lin et al., 2021), however, the permeability is also affected by many factors, for example, effective stress has a significant control effect on the permeability (Lv et al., 2022), when the CO_2 is injected into coal seams at high pressure, the decrease of effective stress has a dominated on permeability and can compensate the permeability loss induced by adsorption swelling (Anggara et al., 2016). Moreover, the moisture, temperature and coal rank are also related to the permeability, their positive and negative effects on the permeability of coal during CO_2 injection have been thoroughly studied (Niu et al., 2019a).

The coal has a complex pore-fracture structure, with the face cleat, butt cleat and bedding plane developing in it (Wang et al., 2018a; Jin et al., 2022; Liu et al., 2022), the permeability thus exhibits strong anisotropic characteristics. The fracture system is the medium to connect the wellbore and the pores in the coal matrix, the anisotropic characteristic of permeability should be emphasized because the permeability in any direction can affect the CO_2 injectivity of coal. To quantitatively describe the permeability of coal, Pan and Connell developed a model to predicate the behavior of anisotropic permeability for primary and enhanced coalbed methane recovery (Pan and Connell, 2011). And lots of investigators have improved the anisotropic permeability model by considering more conditions, such as the temperature (Zhou et al., 2020), the damaging effect (Cheng et al., 2022) and the gas slippage (Chen et al., 2020). However, the dynamic evolution of anisotropic permeability is complex and the evolution mechanism is not clear, meanwhile, the CO_2 injectivity model is lacking and causing the prediction of CO_2 injectivity to be difficult.

Therefore, in this paper, the anisotropic permeability and CO_2 injectivity experiments are first performed by a self-developed CO_2 injection and coalbed methane enhanced development model platform, then the anisotropic permeability evolution characteristics and mechanism are analyzed in depth, and finally, the anisotropic permeability and CO_2 injectivity models are established and verified by the experimental data. This research will provide technical guidance for the efficient CO_2 injection of coal seams and lay the theoretical foundation of CO_2-ECBM.

Experimental work

Sample preparation

The coal samples used in this paper were selected from the Chengzhuang coal mine and Sihe coal mine in Shanxi Province, China. The cubic sample (30 mm × 30 mm × 30 mm) was obtained by cutting from the block coal of Chengzhuang coal mine along the face cleat direction, the butt cleat direction and the bedding plane direction. The cylinder sample (50 mm × 100 mm) was obtained by core drilling rig from the block coal of Sihe coal mine along the vertical bedding direction. Then the

TABLE 1 The basic information of samples used in this work.

Sample source	$R_{o,max}$ (%)	Proximate analysis (wt%)					Ultimate analysis (wt%)			Maceral composition (vol%)		
		M_{ad}	A_{ad}	V_{daf}	FC_{ad}	O_{daf}	C_{daf}	H_{daf}	N_{daf}	Vit	Ine	Min
Chengzhuang coalmine	2.96	2.71	12.18	6.94	81.72	3.27	92.84	2.31	3.27	75.80	21.40	2.80
Sihe coalmine	3.33	1.48	13.12	6.32	81.39	2.98	93.45	2.15	1.00	79.84	18.36	1.80

Note: M_{ad}, moisture content of air-dried basis; A_{ad}, ash content of air-dried basis; V_{daf}, volatile content of dry ash-free basis; FC_{ad}, fixed carbon content of air-dried basis; O_{daf}, oxygen content of dry ash-free basis; C_{daf}, carbon content of dry ash-sfree basis; H_{daf}, hydrogen content of dry ash-free basis; N_{daf}, nitrogen content of dry ash-free basis; Vit, vitrinite; Ine, inertinite; Min, mineral.

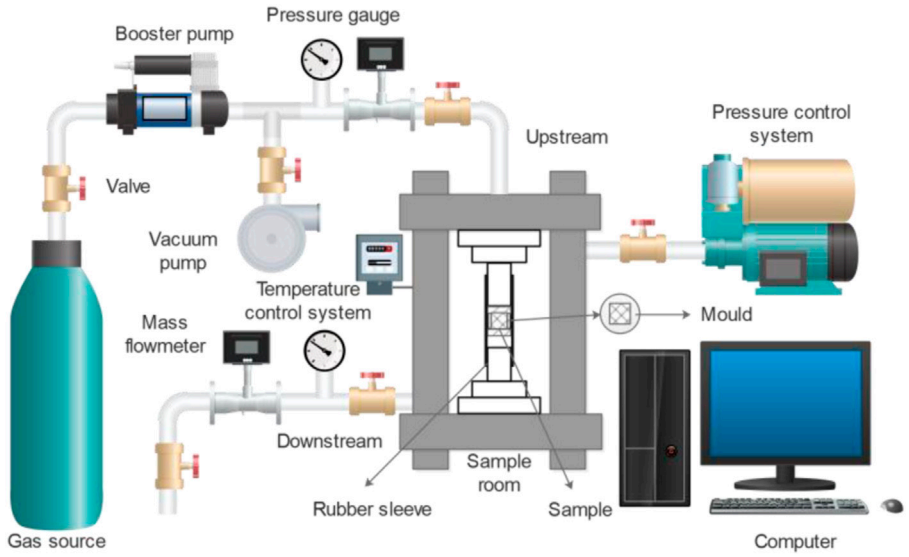

FIGURE 1
The anisotropic permeability testing system.

surfaces of the sample were polished with diamond sandpapers to ensure the accuracy of the experimental results. The proximate analysis, ultimate analysis and maceral composition were measured according to the standards suggested by International Standardization Organization (ISO 589, ISO 562, ISO 1171 and ISO 7404–3) (Table 1). The $R_{o,max}$ of coal samples from Chengzhuang coal mine and Sihe coal mine are 2.96% and 3.33%, respectively, and the fixed carbon, the carbon content and the inertinite are dominant in the results of proximate analysis, ultimate analysis and maceral composition.

Experimental setup

The anisotropic permeability was measured by the testing system shown in Figure 1. The CO_2 is stored in the gas tank and provides the gas source for the whole experimental setup. The booster pump is used to promote the gas pressure to the target value. The pressure gauge and the mass flowmeter are adopted to measure the gas real-time gas pressure and gas flow, with the accuracy of 0.01 MPa and 0.01 ml/min. The temperature control system is employed to guarantee that the experimental setup is still in a state of the constant target temperature. The pressure control system permits independent control of the axial stress and confining pressure of the sample, respectively. The monitored data is transmitted to the computer and the experimental process is operated by the control software installed on the computer. For the measurement of the permeability of the cubic sample, the sample is first installed in the homemade mould and then placed in the rubber sleeve with corrosion resistance, then the anisotropic permeability is tested by changing the sample orientation according to the method by Niu et al. (2018). For the measurement of the permeability of the cylinder sample, the sample is wrapped by

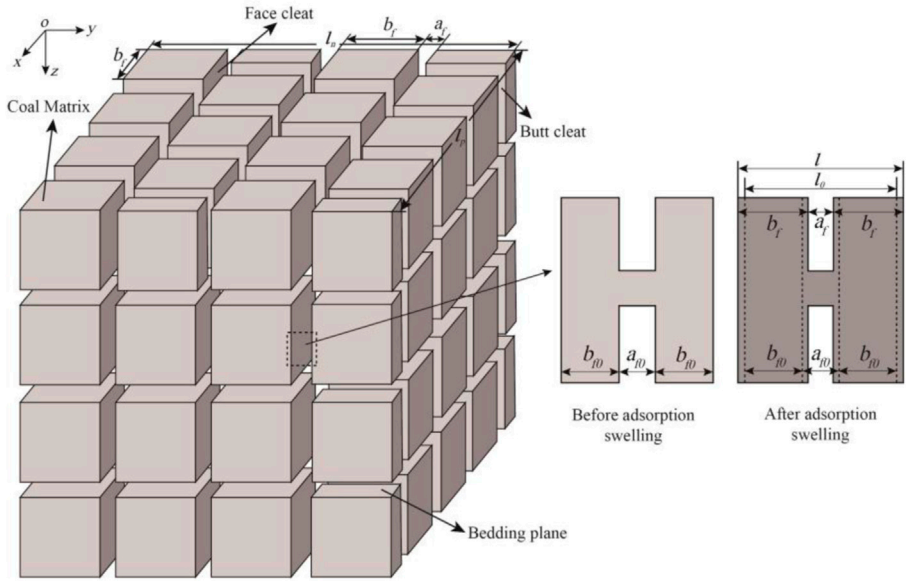

FIGURE 2
Schematic diagram of the representative elementary volume (REV) of coal and adsorption-induced swelling.

a rubber sleeve and placed in the sample room to measure the permeability.

Experimental scheme

The influence of the confining pressure and the gas pressure is analyzed and thus the permeability of coal is measured by alternately changing the confining pressure and the gas pressure. Referring to actual reservoir conditions, the confining pressure is set to 10, 12, 14 and 16 MPa, the gas pressure is set to 1, 2, 3 and 4 MPa, and the temperature is set to 35°C during the whole experimental process. The permeability of coal is calculated by the steady-state method based on the Darcy law, the principle has been introduced in previous research (Niu et al., 2019b; Niu et al., 2020b). For the simulation test of the CO_2 injection process, the confining pressure is 12 MPa, the injection pressure is increased from 2 MPa, 4 MPa, 6 MPa, 8–10 MPa, and the CO_2 injection flow is dynamically monitored by the inlet flowmeter and recorded in the computer.

Anisotropic permeability model of coal during the CO_2 injection process

Model establishment

A large number of studies show that the pores and fractures are widely regularly distributed in coal (Pan et al., 2016; Niu et al., 2017b; Niu et al., 2019a), i.e., the pores with different scales occur in the coal matrix (Jin et al., 2017; Jin et al., 2020), while the fractures occur between the coal matrix and cut coal into a system of matrix blocks. The fractures mainly include the face cleat, the butt cleat and the bedding plane fracture, they are vertically staggered with each other and distributed in the coal body (Rodrigues et al., 2014; Wang et al., 2018b; Jin et al., 2019). For the primary coal without geological structural fractures, the three-dimensional model of coal can be simplified to the representative elementary volume (Figure 2).

The cleats and bedding plane fractures are the main seepage channels, while the permeability of coal has a direct relationship with the porosity (Mckee et al., 1988):

$$\frac{k}{k_0} = \left(\frac{\phi}{\phi_0}\right)^3 \tag{1}$$

where the k and φ represent the permeability and porosity respectively, and the subscript 0 represents the initial value. For the REV, taking the oz direction as an example, the porosity in this direction is the plane porosity degree perpendicular to the oxy section:

$$\phi_f = \frac{A_f}{A_{rz}} \tag{2}$$

where the A_f represents the porosity in the oxy section, A_{rz} represents the area of oxy section. The oxy section is composed of several fractures. Assuming the fracture number is n_f, A_{rz} and A_f can be expressed as:

$$\begin{cases} A_f = n_f a_f l_p \\ A_{rz} = l_n l_p \end{cases} \tag{3}$$

where b_f represents the width of the coal matrix, the width of REV (l_n) is thus composed of fracture width (a_f) and coal matrix width:

$$l_n = (a_f + b_f) n_f \tag{4}$$

Substituting Eqs 3,4 into Eq. 2 to obtain:

$$\phi_f = \frac{A_f}{A_{rz}} = \frac{n_f a_f l_p}{l_n l_p} = \frac{n_f a_f}{(a_f + b_f) n_f} = \frac{a_f}{a_f + b_f} \tag{5}$$

Considering the anisotropic characteristics of coal, the porosity of the face cleat, butt cleat and bedding plane are respectively:

$$\begin{cases} \phi_x = \dfrac{a_x}{a_x + b_x} \\ \phi_y = \dfrac{a_y}{a_y + y} \\ \phi_z = \dfrac{a_z}{a_z + b_z} \end{cases} \tag{6}$$

Taking the face cleat as an example, the derivative of Eq. 6 can be obtained:

$$d\phi_x = d\left(\frac{a_x}{a_x + b_x}\right) = d\left(\frac{l - b_x}{a_x + b_x}\right) = \frac{b_x}{l_x}\left(\frac{dl_x}{l_x} - \frac{db_x}{b_x}\right) \tag{7}$$

Where:

$$\frac{b_x}{l_x} = 1 - \phi_x \tag{8}$$

Substituting Eq. 8 into Eq. 7 to obtain:

$$\frac{d\phi_x}{1 - \phi_x} = \frac{dl_x}{l_x} - \frac{db_x}{b_x} \tag{9}$$

It can also be written as:

$$\frac{\Delta\phi_x}{1 - \phi_x} = \frac{\Delta l_x}{l_x} - \frac{\Delta b_x}{b_x} \tag{10}$$

The porosity of coal is quite low. To simplify the formula, the 1-φ_x is approximated to 1. And the variation of face cleat width is caused by the strain in the direction of the butt cleat, then Eq. 10 can be converted into:

$$\Delta\phi_x = \Delta\varepsilon_y^b - \Delta\varepsilon_y^m \tag{11}$$

The strain of coal is composed of two parts, i.e., the strain caused by the change of effective stress ($\Delta\varepsilon_e$) and the strain caused by gas adsorption ($\Delta\varepsilon_a$), then the strain caused by the change of effective stress and gas adsorption in butt cleat direction are:

$$\begin{cases} \Delta\varepsilon_y^b = \Delta\varepsilon_{ay}^b + \Delta\varepsilon_{ey}^b \\ \Delta\varepsilon_y^m = \Delta\varepsilon_{ay}^m + \Delta\varepsilon_{ey}^m \end{cases} \tag{12}$$

According to Pan and Connell. (2011), for the anisotropic media, the strain caused by the effective stress in the face cleat direction under the action of three-dimensional stress can be expressed as:

$$\begin{cases} \Delta\varepsilon_{ey}^b = \dfrac{\Delta\sigma_{ey} - \nu_{xy}^b \sigma_{ex} - \nu_{zy}^b \sigma_{ez}}{E_y^b} \\ \Delta\varepsilon_{ey}^m = \dfrac{\Delta\sigma_{ey} - \nu_{xy}^m \sigma_{ex} - \nu_{zy}^m \sigma_{ez}}{E_y^m} \end{cases} \tag{13}$$

In this work, the compression is set as negative, the tension is set as positive, and the effective stress of coal is

$$\Delta\sigma_e = \alpha\Delta p - \Delta\sigma_t \tag{14}$$

Where the $\Delta\sigma_t$ represents the change of the external stress, α represents the Biot coefficient, Δp represents the change of the gas pressure. The deformation increment of coal due to gas adsorption is:

$$\begin{aligned} \Delta l &= l - l_0 = a_f + 2b_f - (a_{f0} + 2b_{f0}) \\ &= a_{f0} - 2\Delta\varepsilon_{ain}^m b_{f0} + 2b_{f0}(1 + \Delta\varepsilon_{at}^m) - (a_{f0} + 2b_{f0}) \\ &= 2b_{f0}(\Delta\varepsilon_{at}^m - \Delta\varepsilon_{ain}^m) \end{aligned} \tag{15}$$

Where $\Delta\varepsilon_{at}^m$ represents the total swelling strain change caused by the gas adsorption under limited conditions; $\Delta\varepsilon_{ain}^m$ represents the internal swelling strain change caused by the gas adsorption, which compresses the fractures in the coal and affects the permeability of the coal seam. In combination with Eq. 15, the swelling strain change of coal can be expressed as:

$$\Delta\varepsilon_{at}^b = \frac{\Delta l}{l_0} = \frac{2b_{f0}(\Delta\varepsilon_{at}^m - \Delta\varepsilon_{ain}^m)}{a_{f0} + 2b_{f0}} \tag{16}$$

Since the fracture width in coal is far smaller than the size of the coal matrix, i.e., $a_{f0} \ll b_{f0}$ Eq. 16 can be rewritten as:

$$\Delta\varepsilon_{at}^b = \frac{\Delta l}{l_0} = \frac{2b_{f0}(\Delta\varepsilon_{at}^m - \Delta\varepsilon_{ain}^m)}{a_{f0} + 2b_{f0}} \approx \Delta\varepsilon_{at}^m - \Delta\varepsilon_{ain}^m \tag{17}$$

The measured swelling strain change is $\Delta\varepsilon_{at}^b$ and the internal swelling strain is difficult to measure directly. Therefore, the internal swelling coefficient (f_{in}) is introduced in this paper, which is the ratio of internal swelling strain to total swelling strain. In addition to the influence of gas adsorption, the temperature and moisture will affect the permeability by affecting the internal swelling coefficient of coal. Therefore, assuming that f_{ina}, f_{inT} and f_{inw} are the internal swelling coefficients caused by gas adsorption, temperature and moisture respectively, the total internal swelling coefficient is:

$$f_{in} = f_{ina} + f_{inT} + f_{inw} \tag{18}$$

Then Eq. 17 can be converted into:

$$\Delta\varepsilon_{at}^{b} = \Delta\varepsilon_{at}^{m} - \Delta\varepsilon_{ain}^{m} = \varepsilon_{at}^{m} - \varepsilon_{ai0}^{m} - \left(\varepsilon_{ain}^{m} - \varepsilon_{ai0}^{m}\right) = \varepsilon_{at}^{m} - \varepsilon_{at0}^{m} - \left(f_{in}\varepsilon_{at}^{m} - f_{in0}\varepsilon_{at0}^{m}\right) = \varepsilon_{at}^{m}\left(1 - f_{in}\right) - \varepsilon_{at0}^{m}\left(1 - f_{in0}\right) \tag{19}$$

The change of swelling strain caused by gas adsorption in the face cleat can be expressed as:

$$\Delta\varepsilon_{ay}^{b} = \varepsilon_{ay}^{m}\left(1 - f_{in}\right) - \varepsilon_{ayo}^{m}\left(1 - f_{in0}\right) \tag{20}$$

The matrix swelling of coal conforms to the Langmuir-type equation, then the strain of matrix caused by gas adsorption of face cleat is:

$$\Delta\varepsilon_{ay}^{m} = \frac{\varepsilon_{Ly}P}{P + P_{Ly}} \tag{21}$$

Taking Eqs. 12, 13, 18, 20, and 21 with Eq. 11, the variation of porosity of face cleat is:

$$\Delta\phi_X = \frac{\Delta\sigma_{ey} - \nu_{xy}^{b}\sigma_{ex} - \nu_{zy}^{b}\sigma_{ez}}{E_y^{b}} - \frac{\Delta\sigma_{ey} - \nu_{xy}^{m}\sigma_{ex} - \nu_{zy}^{m}\sigma_{ez}}{E_y^{m}} - \varepsilon_{Ly}\left(\frac{\left(f_{ina} + f_{inT} + f_{inw}\right)_x P}{P + P_{Ly}} - \frac{\left(f_{ina} + f_{inT} + f_{inw}\right)_{x0} P_0}{P_0 + P_{Ly}}\right) \tag{22}$$

In the same way, the variation of porosity of the butt cleat and bedding plane is as follows:

$$\Delta\phi_y = \frac{\Delta\sigma_{ex} - \nu_{yx}^{b}\sigma_{ey} - \nu_{zx}^{b}\sigma_{ez}}{E_x^{b}} - \frac{\Delta\sigma_{ex} - \nu_{yx}^{m}\sigma_{ey} - \nu_{zx}^{m}\sigma_{ez}}{E_x^{m}} - \varepsilon_{Lx}\left(\frac{\left(f_{ina} + f_{inT} + f_{inw}\right)_y P}{P + P_{Lx}} - \frac{\left(f_{ina} + f_{inT} + f_{inw}\right)_{y0} P_0}{P_0 + P_{Lx}}\right) \tag{23}$$

$$\Delta\phi_z = \frac{\Delta\sigma_{ez} - \nu_{yz}^{b}\sigma_{ey} - \nu_{xz}^{b}\sigma_{ex}}{E_z^{b}} - \frac{\Delta\sigma_{ez} - \nu_{yz}^{m}\sigma_{ey} - \nu_{xz}^{m}\sigma_{ex}}{E_z^{m}} - \varepsilon_{Lz}\left(\frac{\left(f_{ina} + f_{inT} + f_{inw}\right)_x P}{P + P_{Lz}} - \frac{\left(f_{ina} + f_{inT} + f_{inw}\right)_{z0} P_0}{P_0 + P_{Lz}}\right) \tag{24}$$

Therefore, the porosity in any seepage direction is:

$$\phi_i = \phi_{i0} + \begin{bmatrix} \frac{\Delta\sigma_{ej} - \nu_{ij}^{b}\Delta\sigma_{ei} - \nu_{kj}^{b}\Delta\sigma_{ek}}{E_j^{b}} - \frac{\Delta\sigma_{ej} - \nu_{ij}^{m}\Delta\sigma_{ei} - \nu_{kj}^{m}\Delta\sigma_{ek}}{E_j^{m}} \\ + \frac{\Delta\sigma_{ek} - \nu_{ik}^{b}\Delta\sigma_{ei} - \nu_{jk}^{b}\Delta\sigma_{ej}}{E_k^{b}} - \frac{\Delta\sigma_{ek} - \nu_{ik}^{m}\Delta\sigma_{ei} - \nu_{jk}^{m}\Delta\sigma_{ej}}{E_k^{m}} \\ -\varepsilon_{Lj}\left(\frac{\left(f_{ina} + f_{inT} + f_{inw}\right)_j P}{P + P_{Lj}} - \frac{\left(f_{ina} + f_{inT} + f_{inw}\right)_{j0} P_0}{P + P_{Lj}}\right) \\ -\varepsilon_{Lk}\left(\frac{\left(f_{ina} + f_{inT} + f_{inw}\right)_k P}{P + P_{Lk}} - \frac{\left(f_{ina} + f_{inT} + f_{inw}\right)_{k0} P_0}{P_0 + P_{Lk}}\right) \end{bmatrix} \tag{25}$$

Substitute Eq. 25 into Eq. 1 to obtain:

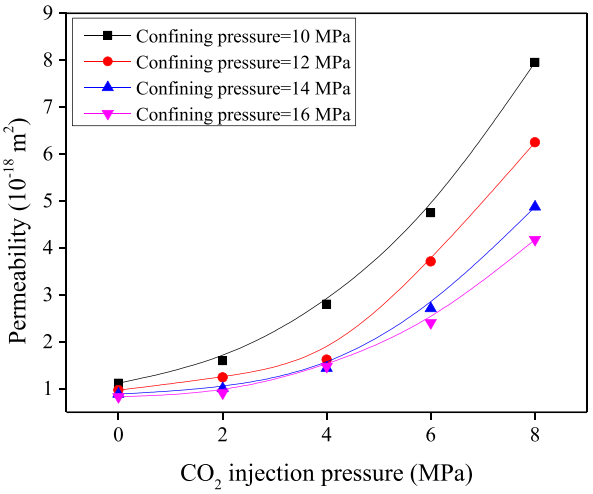

FIGURE 3
Changes in the permeability of cylinder sample with the increasing CO_2 injection pressure.

$$k_i = k_{i0}\left\{1 + \frac{1}{\phi_{i0}}\begin{bmatrix} \frac{\Delta\sigma_{ej} - \nu_{ij}^{b}\Delta\sigma_{ei} - \nu_{kj}^{b}\Delta\sigma_{ek}}{E_j^{b}} - \frac{\Delta\sigma_{ej} - \nu_{ij}^{m}\Delta\sigma_{ei} - \nu_{kj}^{m}\Delta\sigma_{ek}}{E_j^{m}} \\ + \frac{\Delta\sigma_{ek} - \nu_{ik}^{b}\Delta\sigma_{ei} - \nu_{jk}^{b}\Delta\sigma_{ej}}{E_k^{b}} - \frac{\Delta\sigma_{ek} - \nu_{ik}^{m}\Delta\sigma_{ei} - \nu_{jk}^{m}\Delta\sigma_{ej}}{E_k^{m}} \\ -\varepsilon_{Lj}\left(\frac{\left(f_{ina} + f_{inT} + f_{inw}\right)_j P}{P + P_{Lj}} - \frac{\left(f_{ina} + f_{inT} + f_{inw}\right)_{j0} P_0}{P + P_{Lj}}\right) \\ -\varepsilon_{Lk}\left(\frac{\left(f_{ina} + f_{inT} + f_{inw}\right)_k P}{P + P_{Lk}} - \frac{\left(f_{ina} + f_{inT} + f_{inw}\right)_{k0} P_0}{P_0 + P_{Lk}}\right) \end{bmatrix}^3\right\} \tag{26}$$

Where, $i \neq j \neq k$, for coal with a porous structure, the elastic modulus of the matrix is far greater than that of coal, i.e., $E_j^{m} \gg E_j^{b}$, Eq. 26 is converted into:

$$k_i = k_{i0}\left\{1 + \frac{1}{\phi_{i0}}\begin{bmatrix} \frac{\Delta\sigma_{ej} - \nu_{ij}^{b}\Delta\sigma_{ei} - \nu_{kj}^{b}\Delta\sigma_{ek}}{E_j^{b}} + \frac{\Delta\sigma_{ek} - \nu_{ik}^{m}\Delta\sigma_{ei} - \nu_{jk}^{m}\Delta\sigma_{ej}}{E_j^{m}} \\ -\varepsilon_{Lj}\left(\frac{\left(f_{ina} + f_{inT} + f_{inw}\right)_j P}{P + P_{Lj}} - \frac{\left(f_{ina} + f_{inT} + f_{inw}\right)_{j0} P_0}{P_0 + P_{Lj}}\right) \\ -\varepsilon_{Lk}\left(\frac{\left(f_{ina} + f_{inT} + f_{inw}\right)_k P}{P + P_{Lk}} - \frac{\left(f_{ina} + f_{inT} + f_{inw}\right)_{k0} P_0}{P_0 + P_{Lk}}\right) \end{bmatrix}^3\right\} \tag{27}$$

Boundary condition

(1) Constant confining pressure

Under this boundary condition, the pore pressure changes while the total stress remains unchanged:

$$\Delta\sigma_{tx} = \Delta\sigma_{ty} = \Delta\sigma_{tz} = 0 \tag{28}$$

The effective stress can be expressed as:

$$\Delta\sigma_{ex} = \Delta\sigma_{ey} = \Delta\sigma_{ez} = \Delta P \tag{29}$$

Substitute Eq. 29 into Eq. 27 to obtain the permeability model under the boundary condition of constant confining pressure:

$$k_i = k_{i0}\left\{1 + \frac{1}{\phi_{i0}}\left[\begin{array}{l} \frac{\left(1-V_{ij}^b-V_{kj}^b\right)\Delta P}{E_j^b} + \frac{\left(1-V_{ik}^b-V_{jk}^b\right)\Delta P}{E_k^b} \\ -\varepsilon_{Lj}\left(\frac{\left(f_{ina}+f_{inT}+f_{inw}\right)_j P}{P+P_{Lj}} - \frac{\left(f_{ina}+f_{inT}+f_{inw}\right)_{j0}P_0}{P_0+P_{Lj}}\right) \\ -\varepsilon_{Lk}\left(\frac{\left(f_{ina}+f_{inT}+f_{inw}\right)_k P}{P+P_{Lk}} - \frac{\left(f_{ina}+f_{inT}+f_{inw}\right)_{k0}P_0}{P_0+P_{Lk}}\right) \end{array}\right]\right\}^3 \tag{30}$$

(2) Constant effective stress

Under this boundary condition, the effective stress remains unchanged, i.e., the increment of the effective stress is always zero:

$$\Delta\sigma_{ex} = \Delta\sigma_{ey} = \Delta\sigma_{ez} = 0 \tag{31}$$

Substitute Eq. 31 into Eq. 27 to obtain the permeability model under the boundary condition of constant effective stress:

$$k_i = k_{i0}\left\{1 - \frac{1}{\phi_{i0}}\left[\begin{array}{l} -\varepsilon_{Lj}\left(\frac{\left(f_{ina}+f_{inT}+f_{inw}\right)_j P}{P+P_{Lj}} - \frac{\left(f_{ina}+f_{inT}+f_{inw}\right)_{j0}P_0}{P_0+P_{Lj}}\right) \\ +\varepsilon_{Lk}\left(\frac{\left(f_{ina}+f_{inT}+f_{inw}\right)_k P}{P+P_{Lk}} - \frac{\left(f_{ina}+f_{inT}+f_{inw}\right)_{k0}P_0}{P_0+P_{Lk}}\right) \end{array}\right]\right\}^3 \tag{32}$$

(3) Constant pore pressure

Under this boundary condition, the pore pressure remains unchanged, i.e., the increment of pore pressure is constant at zero:

$$\Delta P = 0 \tag{33}$$

The effective stress formula can be changed to:

$$\Delta\sigma_e = -\Delta\sigma_t \tag{34}$$

Substitute Eq. 34 into Eq. 27 to obtain the permeability model under the boundary condition of constant pore pressure:

$$k_i = k_{i0}\left\{1 - \frac{1}{\phi_{i0}}\left[\begin{array}{l} \frac{\Delta\sigma_{tj}-v_{ij}^b\Delta\sigma_{ti}-v_{kj}^b\Delta\sigma_{tk}}{E_j^b} + \frac{\Delta\sigma_{tk}-v_{ik}^b\Delta\sigma_{ti}-v_{jk}^b\Delta\sigma_{tj}}{E_j^m} \\ +\varepsilon_{Lj}\left(\frac{\left(f_{ina}+f_{inT}+f_{inw}\right)_j - \left(f_{ina}+f_{inT}+f_{inw}\right)_{j0}P_0}{P+P_{Lj}}\right) \\ +\varepsilon_{Lk}\left(\frac{\left(f_{ina}+f_{inT}+f_{inw}\right)_k - \left(f_{ina}+f_{inT}+f_{inw}\right)_{k0}P_0}{P_0+P_{Lk}}\right) \end{array}\right]\right\}^3 \tag{35}$$

Results and discussion

Permeability and model validation of cylinder sample

The permeability of the cylinder sample under different CO_2 injection pressures and confining pressures is shown in Figure 3. When the CO_2 injection pressure increases from 2 to 8 MPa, the permeability averagely increases from 0.95 $m^2 \times 10^{-18}$ m^2 to 5.81 $m^2 \times 10^{-18}$ m^2; when the confining pressure increases from 10 to 16 MPa, the permeability averagely decreases from 3.64 $m^2 \times 10^{-18}$ m^2 to 1.96 $m^2 \times 10^{-18}$ m^2. Apparently, the CO_2 permeability of coal is positively related to the injection pressure and negatively related to the confining pressure. Increasing the confining pressure will compress the fractures developed in coal and reduce the permeability while increasing the injection pressure will decrease the effective stress and promote the permeability.

For the cylinder sample, the permeability is assumed to be isotropic, hence, and Eq. 36 can be transformed into:

$$v_{ij}^b = v_{ik}^b = v_{ik}^b = v^b, E_j^b = E_k^b = E^b \tag{36}$$

$$k_i = k_{i0}\left\{1 - \frac{1}{\phi_{i0}}\left[\frac{2\left(1-2v^b\right)\Delta P}{E^b} - \varepsilon_L\left(\begin{array}{l} \frac{\left(f_{ina}+f_{inT}+f_{inw}\right)P}{P+P_{Lj}} \\ -\frac{\left(f_{ina}+f_{inT}+f_{inw}\right)_0 P_0}{P_0+P_{Lj}} \end{array}\right)\right]\right\}^3 \tag{37}$$

To verify the reliability of the proposed model, the relevant parameters are from the literature (Peng et al., 2017), as shown in Table 2. The experimental data for permeability were first converted to k/k_0 and then fitted by the permeability model (Figure 4). The experimental data has a high correlation with this model, the correlation coefficients are all greater than 0.99. It indicates that the anisotropic permeability model can be used to predict the change of isotropic permeability if the difference of mechanical parameters in different directions is ignored. It can be seen that the k/k_0 gradually increases with the increase of CO_2 injection pressure. This is because the CO_2 injection causes the closed fractures to reopen. At the same time, the coal matrix swells to the outside, resulting in the widening of the fractures and improving the permeability of coal.

Permeability and model validation of cubic sample

The permeability of the cubic sample under different CO_2 injection pressures and confining pressures is shown in Figure 5. As a whole, the variation trends of permeability in either direction with confining pressure and CO_2 injection pressure are coincident, this indicates that the influence of the effect stress on the seepage capacity of face cleat, butt cleat and bedding plane fracture is analogous. However, the permeability measured in different directions shows distinct anisotropic characteristics. The ratios of k_x:k_y:k_z are 1.53:1.35:1, 1.58:1.42:1, 1.58:1.33:1, and 1.61:1.43:1 respectively, e.g., the permeability of coal in parallel face cleat direction is the largest, followed by the permeability of coal in parallel butt cleat direction, and that in vertical bedding direction is the minimum. The k_x, k_y and k_z of coal are respectively

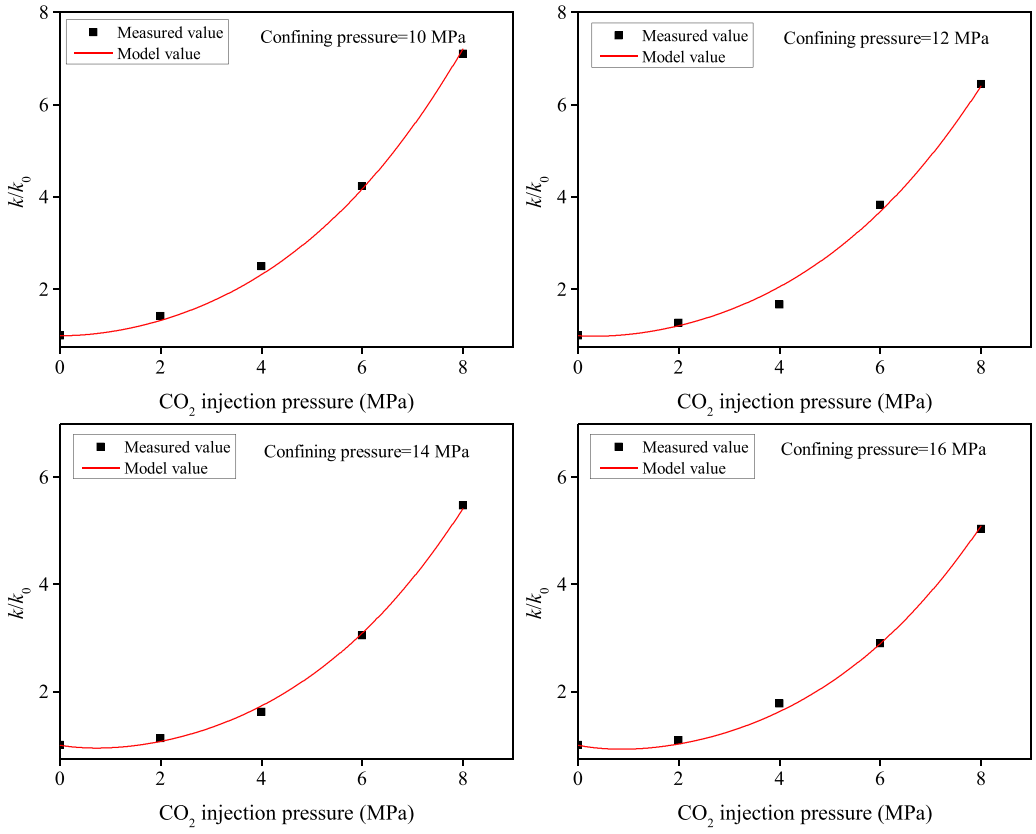

FIGURE 4
Fitting results of the permeability results of cylinder sample.

TABLE 2 Parameter values used for model validation of permeability of cylinder sample.

Parameter	Value	Unit
E^b	1,300	MPa
ν^b	0.3	—
ϕ_0	0.3	%
p_0	0	MPa
p_L	6	MPa
ε_L	0.025	—

contributed by the "face cleat + bedding plane fracture", the "butt cleat and bedding plane fracture" and the "bedding plane fracture", generally, the sequence of the average aperture from large to small is bedding plane fracture, face cleat and butt cleat (Busse et al., 2017; Shi et al., 2018; Wang et al., 2019). According to the parallel-plate law of fractures (Klimczak et al., 2010), it can be deduced that the permeability distribution in the different directions measured in this paper is reasonable and correct.

To verify the correctness of the anisotropic permeability model proposed in this paper, the parameters of elastic modulus, Poisson's ratio, Langmuir strain and Langmuir pressure were selected from the previous literatures and the porosity was the assumed value. The elastic modulus, Langmuir strain and Langmuir pressure are considered isotropic in the parallel bedding plane direction, while the Poisson's ratio is considered isotropic in three directions. The permeability results of the cubic sample are fitted by Eq. 38, it can be seen that the model value and the measured value show the same change trend (Figure 6), their correlation coefficients are higher than 0.96. Obviously, this anisotropic permeability model can be appropriate to evaluate the permeability evolution of heterogeneous coal reservoirs with CO_2 injection under *in situ* conditions.

CO_2 injectivity characteristic of coal

As analyzed above, CO_2 injectivity is the most critical factor restricting the implementation of CO_2-ECBM projects. To

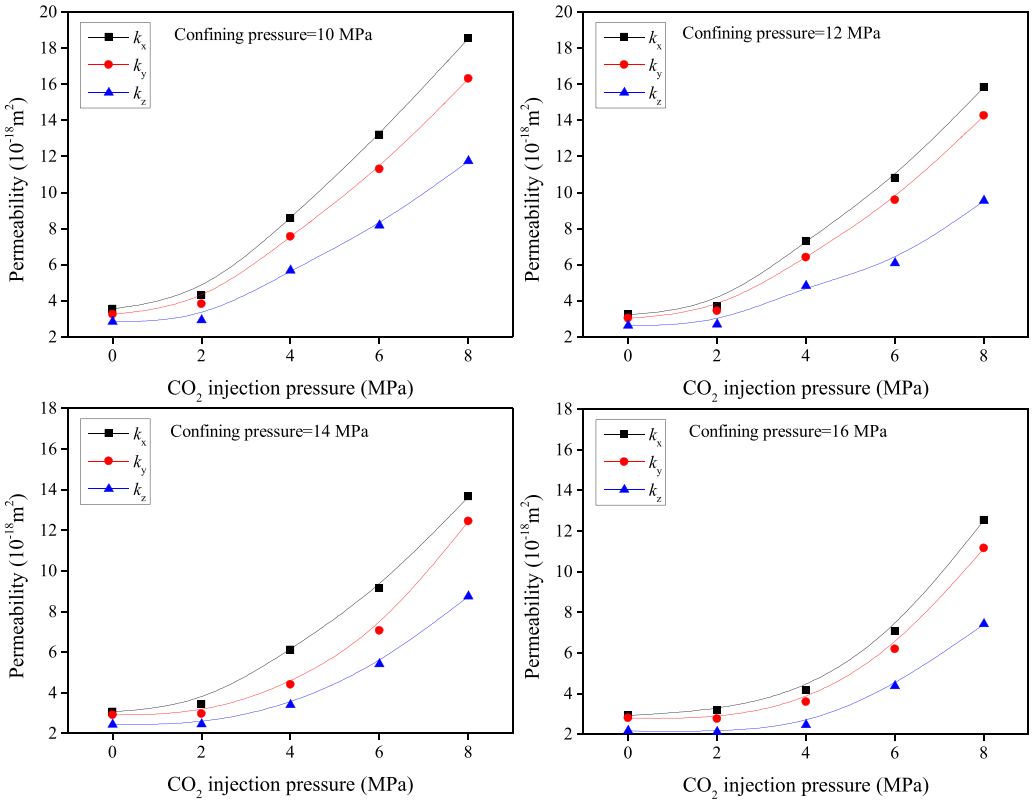

FIGURE 5
Changes in the permeability of cubic sample with the increasing CO_2 injection pressure.

investigate the CO_2 injectivity, the parameter of injectivity rate (J) is used to characterize the CO_2 injectivity of coal (Heddle et al., 2003):

$$J = \frac{Q_{in}}{h(P_{wf} - P)} \tag{38}$$

where h is the coal reservoir thickness, m; p_{wf} is the pressure at the wellbore, MPa; p is the reservoir pressure, MPa; Q_{in} is the injection flow, m^3/d.

The indoor permeability test formula is:

$$k = \frac{2Qp_a\mu L}{A(P_{in}^2 - P_{out}^2)} \tag{39}$$

Where k is the permeability, 10^{-15} m^2, Q is the volumetric rate of flow, cm^3/s; μ is the fluid viscosity, cp; L is the length of the sample, cm; A is the cross-section area of the sample, cm^2, p_{in} is the inlet gas pressure, Pa; p_{out} is the outlet gas pressure, Pa. Q=Q_{in}-V/t, V is the volume of pore in coal (cm^3) and t is the injection time (min).

Thus, the calculation formula for CO_2 injectivity of coal is:

$$J = \frac{kA(P_{in}^2 - P_{out}^2)}{h(P_{wf} - P)P_a\mu L} \tag{40}$$

The equivalent permeability can be expressed as:

$$k = \sqrt[3]{k_x k_y k_z} \tag{41}$$

Combining Eqs. 35, 39 the CO_2 injectivity evaluation model is obtained as follows:

$$J = \frac{A(P_{in}^2 - P_{out}^2)}{h(P_{wf} - P)P_a\mu L}\prod_{i\neq j\neq k}\left\{k_{i0} + \frac{k_{i0}}{\phi_{i0}}\begin{bmatrix} \frac{\Delta\sigma_{ej} - v_{ij}^b\Delta\sigma_{ei} - v_{kj}^b\Delta\sigma_{ek}}{E_j^b} + \frac{\Delta\sigma_{ek} - v_{ik}^b\Delta\sigma_{ei} - v_{jk}^b\Delta\sigma_{ej}}{E_k^b} \\ -\varepsilon_{Lj}\left(\frac{(f_{ina} + f_{inT} + f_{inw})_j}{P_{in} + P_{Lj}} - \frac{(f_{ina} + f_{inT} + f_{inw})_{j0}P_0}{P_0 + P_{Lj}}\right) \\ -\varepsilon_{Lk}\left(\frac{(f_{ina} + f_{inT} + f_{inw})_k P_{in}}{P_{in} + P_{Lk}} - \frac{(f_{ina} + f_{inT} + f_{inw})_{k0}P_0}{P_0 + P_{Lj}}\right) \end{bmatrix}\right\} \tag{42}$$

Then, the CO_2 injectivity evaluation model under the constant confining pressure condition can be converted to:

$$J = \frac{A(P_{in}^2 - P_{out}^2)}{h(P_{wf} - P)P_a\mu L}\prod_{i\neq j\neq k}\left\{k_{i0} + \frac{k_{i0}}{\phi_{i0}}\begin{bmatrix} \frac{(1 - v_{ij}^b - v_{kj}^b)\Delta P}{E_j^b} - \frac{(1 - v_{ik}^b - v_{jk}^b)\Delta P}{E_k^b} \\ -\varepsilon_{Lj}\left(\frac{(f_{ina} + f_{inT} + f_{inw})_j P_{in}}{P + P_{Lj}} - \frac{(f_{ina} + f_{inT} + f_{inw})_{j0}P_0}{P_0 + P_{Lj}}\right) \\ -\varepsilon_{Lk}\left(\frac{(f_{ina} + f_{inT} + f_{inw})_k P}{P + P_{Lk}} - \frac{(f_{ina} + f_{inT} + f_{inw})_{k0}P_0}{P_0 + P_{Lj}}\right) \end{bmatrix}\right\} \tag{43}$$

The changes in instantaneous injectivity rate with the time of coal under the confining pressure of 12 MPa are shown in

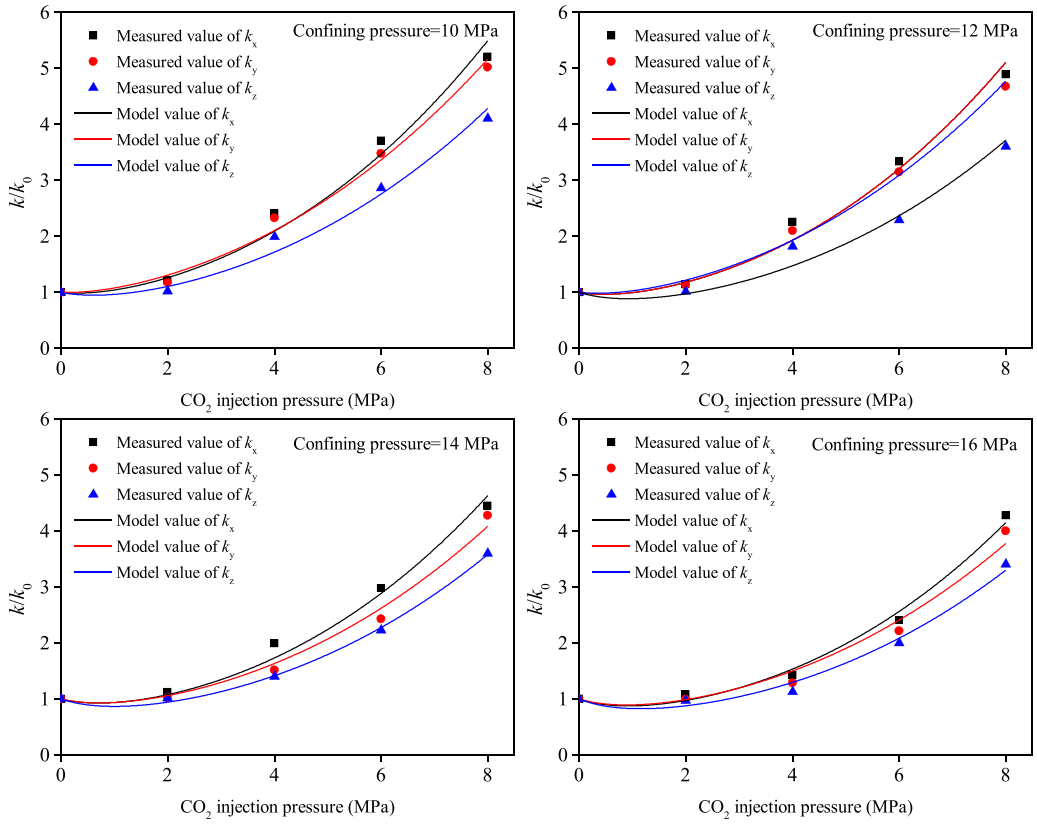

FIGURE 6
Fitting results of the permeability results of cubic sample.

Figure 7. When the CO_2 injection is injected into coal, the instantaneous injectivity rate is advanced immediately and shows several fluctuations. The maximum instantaneous injectivity rate for the subcritical CO_2 (CO_2 injection pressure < 7.4 MPa) can reach 1.8 cm^2/MPa min. The injection pressure is then reduced after 1 h and the CO_2 injectivity cannot recover during the subsequent monitoring process. Compared with the subcritical CO_2, there is no improvement in the instantaneous injectivity rate when the injection pressure reaches 8 MPa, while the maintenance time of the CO_2 injection process is promoted. In particular, two instantaneous injectivity rate peaks appear after 2 h of CO_2 injection. When the CO_2 injection pressure is equal to 10 MPa, the instantaneous injectivity rate increases dramatically, the maximum instantaneous injectivity rate is close to 5 cm^2/MPa min, and the injection process has the longest duration (3 h). It can be seen that the CO_2 injectivity of coal increases with the increase of injection pressure, which is because the closed fractures of coal are effectively supported and reopened under high injection pressure. At the same time, the high reservoir pressure drives more CO_2 molecules to migrate and diffuse into coal pores and further causes the injectivity increase of the coal seam.

Sum the instantaneous injectable rate at each injection pressure to obtain the total CO_2 injectivity rate, the relationship between the total CO_2 injectivity rate and the CO_2 injection pressure is shown in Figure 8 The total CO_2 injectivity rate is nonlinearly increased from 13.61 cm^2/MPa min to 311.87 cm^2/MPa min when the CO_2 injection pressure raises from 2 MPa to 10 MPa. The total CO_2 injectivity rate increases slowly during the subcritical CO_2 injection process and increase quickly during the supercritical CO_2 injection process.

The Formula (45) is used to fit the results between the total injectivity rate and the CO_2 injection pressure, the comparison results of the model value and the measured value are shown in Figure 8. The parameters used in the fitting process are from Table 3, the overall change trend of the CO_2 injectivity evaluation model is consistent with the experimental value. The main reason for the inconsistency depends on the selection of parameters and supposed conditions. Despite all this, the proposed CO_2 injectivity evaluation model is capable of predicting the CO_2 injectivity of a coal seam and will guide the favorable area optimization of CO_2-ECBM.

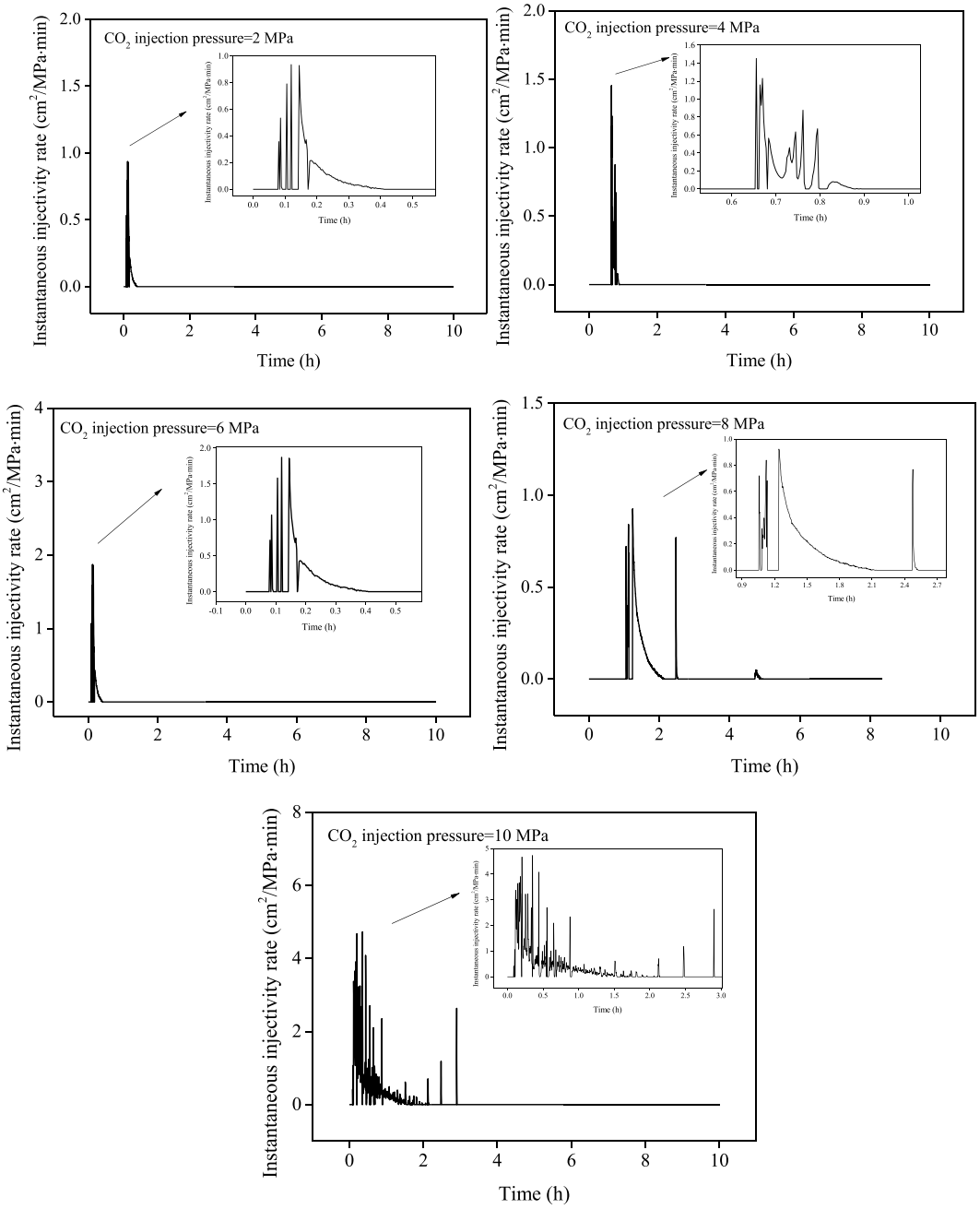

FIGURE 7
Changes in instantaneous injectivity rate with time.

Analysis of improving CO_2 injectivity of coal

CO_2 injectivity is the first requirement for evaluating the effectiveness of CO_2-ECBM, the main reason for CO_2-ECBM not being carried out on a large scale in China is that the CO_2 is difficult to be injected into coal seams. The key to restricting CO_2 injectivity is the permeability reduction induced by the adsorption swelling of the coal matrix. While the cleats are more susceptible to the swelling strain compared with the bedding plane fractures or other larger structural fractures (Niu et al., 2018), therefore, the narrowing or closing of the cleats intercepts the continuous injection process of CO_2 from the wellbores to the coal matrix pores. And both our experiment

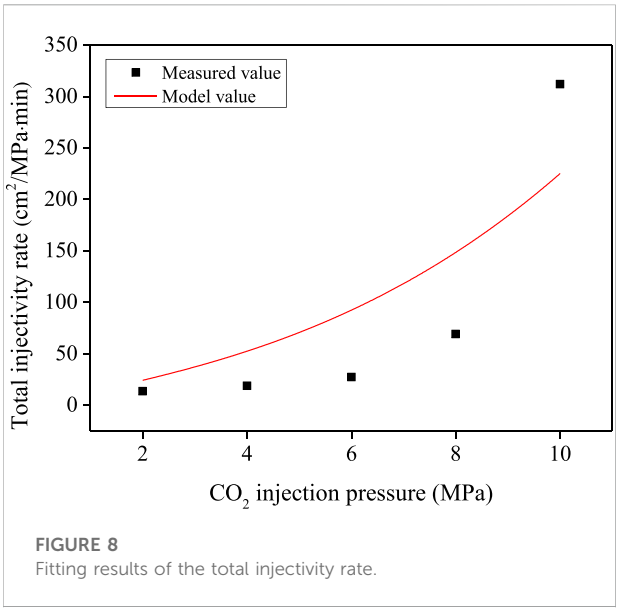

FIGURE 8
Fitting results of the total injectivity rate.

TABLE 3 Parameter values used for model validation of permeability of cubic sample.

Parameter	Value	Unit	Data source
$E_x^b = E_y^b$	2,800	MPa	Zhao et al. (2014)
E_z^b	2,120	MPa	
$\nu_x = \nu_y = \nu_z$	0.24	—	Jia, (2016)
ϕ_{x0}	0.340	%	Experimental value
ϕ_{y0}	0.350	%	
ϕ_{z0}	0.295	%	
$\varepsilon_{Lx}=\varepsilon_{Ly}$	0.634	%	Wang et al. (2013)
ε_{Lz}	1.063	%	
$p_{Lx} = p_{Ly}$	2.707	MPa	
p_{Lz}	2.582	MPa	

and numerical simulation confirm that increasing the CO_2 injection pressure can first offset the permeability decrease induced by adsorption swelling and then promote the permeability, this positive effect may be more favorable for the larger fractures and has little effect on the cleats (Zhang et al., 2019). Thus, increasing the CO_2 injection pressure may temporarily promote CO_2 injectivity, while the CO_2 injection increment is limited.

In the previous research, the intermittent CO_2 injection, N_2 displacing CO_2 and pre-fracturing for improving CO_2 injectivity were validated by the indoor experiment (Niu et al., 2021b), the reservoir stimulation may be the direct and effective measures to solve the problem of CO_2 injectivity attenuation. While traditional hydraulic fracturing can induce large-scale fractures and cannot connect the fractures on the cleat scale. The high-pressure CO_2 gas fracturing can damage the coal seams and promote the formation of the complex network of micro-fractures (Cao et al., 2022), which may promote the cleat seepage of coal during the CO_2 injection process and then increase the CO_2 injectivity. Thus, the CO_2 fracturing by phase transition may be available for enhancing the CO_2 injection and should be focused on in the future.

Conclusion

In this paper, the anisotropic permeability and CO_2 injectivity of coal during CO_2 enhanced coalbed methane recovery process were measured, and the corresponding numerical models were established and verified by the experimental data. Based on this, the dynamic evolution of CO_2 injectivity and methods of improving CO_2 injectivity was clarified. The major conclusions are drawn as follows:

(1) The anisotropic permeability of coal during the CO_2 injection process can be measured by the cubic coal samples. The permeability of coal in parallel face cleat direction is the largest, followed by the permeability of coal in parallel butt cleat direction, and that in vertical bedding direction is the minimum. The ratios of k_x:k_y:k_z are 1.53:1.35:1, 1.58:1.42:1, 1.58:1.33:1, and 1.61:1.43:1 respectively when the CO_2 injection pressure increases from 10 MPa to 16 MPa. The CO_2 injectivity is transformed from the data of CO_2 inlet flow, with the increase of the CO_2 injection pressure, the peak value of instantaneous injectivity rate is enhanced and the injection time is prolonged. The total CO_2 injectivity rate is nonlinearly increased from 13.61 cm^2/MPamin to 311.87 cm^2/MPamin when the CO_2 injection pressure raises from 2 to 10 MPa.

(2) The anisotropic permeability model of coal considering the influence of adsorption swelling, effective stress, water and temperature are established, the injectivity rate is proposed to describe the CO_2 injectivity of coal and the CO_2 injectivity prediction model is built based on the anisotropic permeability model. The validity of these models is confirmed by the experimental results in this paper.

(3) The narrowing or closing of the cleats during the CO_2 injection process intercept the continuous injection process of CO_2 from the wellbores to coal matrix pores. Increasing the CO_2 injection pressure may temporarily promote CO_2 injectivity, while the CO_2 injection increment is limited. The CO_2 fracturing by phase transition may be effective for connecting the cleats in coal, which is thus an available reservoir stimulation method for enhancing the CO_2 injection and should be focused on in the future.

Data availability statement

The datasets presented in this study can be found in online repositories. The names of the repository/repositories and accession number(s) can be found in the article/Supplementary Material.

Author contributions

Writing—original draft: QN; conceptualization: WW; methodology: MH and BL; validation: XH and WS; formal analysis: QW; visualization: JC; resources: ZJ; supervision: XQ.

Funding

This work was supported by the National Natural Science Foundation of China (U1967208, 51979170, and 11902208), the Hebei Natural Science Foundation (E2021210128, E2021210077, and E2020208071), the S&T Program of Hebei (22374102D and 216Z5403G), the Science and Technology Project of Hebei Education Department (QN2021129 and BJK2022010), the Autonomous Subject of State Key Laboratory of Mechanical Behavior and System Safety of Traffic Engineering Structures (KF2020-08), and the Natural Science Foundation of Henan (222300420366).

Conflict of interest

Author BL was employed by the company CNPC Bohai Drilling Engineering Co., Ltd., and PetroChina. Author XH was employed by the company Changqing Oilfield Company and PetroChina Company Limited. Author WS was employed by the company Exploration Division of Changqing Oilfield Company, PetroChina Company Limited.

The remaining authors declare that the research was conducted in the absence of any commercial or financial relationships that could be construed as a potential conflict of interest.

Publisher's note

References

Anggara, F., Sasaki, K., and Sugai, Y. (2016). The correlation between coal swelling and permeability during CO_2 sequestration: A case study using kushiro low rank coals. *Int. J. Coal Geol.* 166, 62–70. doi:10.1016/j.coal.2016.08.020

Busse, J., de Dreuzy, J. R., Galindo Torres, S., Bringemeier, D., and Scheuermann, A. (2017). Image processing based characterisation of coal cleat networks. *Int. J. Coal Geol.* 169, 1–21. doi:10.1016/j.coal.2016.11.010

Cao, Y., Zhang, J., Zhang, X., Liu, S., and Elsworth, D. (2022). Micro-fractures in coal induced by high pressure CO_2 gas fracturing. *Fuel* 311, 122148. doi:10.1016/j.fuel.2021.122148

Chen, Y., Jiang, C., Leung, J. Y., Wojtanowicz, A. K., and Zhang, D. (2020). Gas slippage in anisotropically-stressed shale: An experimental study. *J. Petroleum Sci. Eng.* 195, 107620. doi:10.1016/j.petrol.2020.107620

Cheng, X., Chen, L., Luan, H., Zhang, J., and Jiang, Y. (2022). Why coal permeability changes under unconstrained displacement boundary conditions: Considering damage effects. *J. Nat. Gas Sci. Eng.* 105, 104702. doi:10.1016/j.jngse.2022.104702

Godec, M., Koperna, G., and Gale, J. (2014). CO_2-ECBM: A review of its status and global potential. *Energy Procedia* 63, 5858–5869. doi:10.1016/j.egypro.2014.11.619

Heddle, G., Herzog, H., and Klett, M. (2003). *The economics of CO_2 storage*. Massachusetts Institute of Technology, Laboratory for Energy and the Environment.

Janzen, R., Davis, M., and Kumar, A. (2020). Evaluating long-term greenhouse gas mitigation opportunities through carbon capture, utilization, and storage in the oil sands. *Energy* 209, 118364. doi:10.1016/j.energy.2020.118364

Jia, J. L. (2016). *Experimental simulation on stress and StrainEffects as supercritical CO_2 being injected into deep anthracite reservoirs*. Xuzhou: China University of Mining and Technology.

Jin, Y., Dong, J., Zhang, X., Li, X., and Wu, Y. (2017). Scale and size effects on fluid flow through self-affine rough fractures. *Int. J. Heat Mass Transf.* 105, 443–451. doi:10.1016/j.ijheatmasstransfer.2016.10.010

Jin, Y., Wang, C., Liu, S., Quan, W., and Liu, X. (2020). Systematic definition of complexity assembly in fractal porous media. *Fractals* 28, 2050079. doi:10.1142/s0218348x20500796

Jin, Y., Zheng, J., Dong, J., Wang, Q., Liu, Y., Wang, B., et al. (2022). Fractal topography and complexity assembly in multifractals. *Fractals* 30, 529. doi:10.1142/s0218348x22500529

Jin, Y., Zheng, J., Liu, X., Pan, J., and Liu, S. (2019). Control mechanisms of self-affine, rough cleat networks on flow dynamics in coal reservoir. *Energy* 189, 116146. doi:10.1016/j.energy.2019.116146

Klimczak, C., Schultz, R. A., Parashar, R., and Reeves, D. M. (2010). Cubic law with aperture-length correlation: Implications for network scale fluid flow. *Hydrogeol. J.* 18, 851–862. doi:10.1007/s10040-009-0572-6

Kumar, H., Elsworth, D., Liu, J., Pone, D., and Mathews, J. P. (2012). Optimizing enhanced coalbed methane recovery for unhindered production and CO_2 injectivity. *Int. J. Greenh. Gas Control* 11, 86–97. doi:10.1016/j.ijggc.2012.07.028

Lin, J., Ren, T., Cheng, Y., and Nemcik, J. (2021). Laboratory quantification of coal permeability reduction effect during carbon dioxide injection process. *Process Saf. Environ. Prot.* 148, 638–649. doi:10.1016/j.psep.2021.01.038

Liu, X., Nie, B., Guo, K., Zhang, C., Wang, Z., and Wang, L. (2021). Permeability enhancement and porosity change of coal by liquid carbon dioxide phase change fracturing. *Eng. Geol.* 287, 106106. doi:10.1016/j.enggeo.2021.106106

Liu, X., Wang, L., Kong, X., Ma, Z., Nie, B., Song, D., et al. (2022). Role of pore irregularity in methane desorption capacity of coking coal. *Fuel* 314, 123037. doi:10.1016/j.fuel.2021.123037

Lv, A., Ali Aghighi, M., Masoumi, H., and Roshan, H. (2022). On swelling stress-strain of coal and their interaction with external stress. *Fuel* 311, 122534. doi:10.1016/j.fuel.2021.122534

Mckee, C. R., Bumb, A. C., and Koenig, R. A. (1988). Stress-Dependent permeability and porosity of coal and other geologic formations. *SPE Form. Eval.* 3, 81–91. doi:10.2118/12858-pa

Niu, Q., Cao, L., Sang, S., Wang, W., Yuan, W., Chang, J., et al. (2021b). A small-scale experimental study of CO_2 enhanced injectivity methods of the high-rank coal. *Petroleum Sci.* 18, 1427–1440. doi:10.1016/j.petsci.2021.08.006

Niu, Q., Cao, L., Sang, S., Wang, W., Zhou, X., Yuan, W., et al. (2021a). Experimental study on the softening effect and mechanism of anthracite with CO_2 injection. *Int. J. Rock Mech. Min. Sci.* 138, 104614. doi:10.1016/j.ijrmms.2021.104614

Niu, Q., Cao, L., Sang, S., Zhou, X., and Liu, S. (2019a). Experimental study of permeability changes and its influencing factors with CO_2 injection in coal. *J. Nat. Gas Sci. Eng.* 61, 215–225. doi:10.1016/j.jngse.2018.09.024

Niu, Q., Cao, L., Sang, S., Zhou, X., Wang, W., Yuan, W., et al. (2020a). Study on the anisotropic permeability in different rank coals under influences of supercritical CO_2 adsorption and effective stress and its enlightenment for CO_2 enhance coalbed methane recovery. *Fuel* 262, 116515. doi:10.1016/j.fuel.2019.116515

Niu, Q., Cao, L., Sang, S., Zhou, X., and Wang, Z. (2018). Anisotropic adsorption swelling and permeability characteristics with injecting CO_2 in coal. *Energy fuels.* 32, 1979–1991. doi:10.1021/acs.energyfuels.7b03087

Niu, Q., Cao, L., Sang, S., Zhou, X., Wang, Z., and Wu, Z. (2017a). The adsorption-swelling and permeability characteristics of natural and reconstituted anthracite coals. *Energy* 141, 2206–2217. doi:10.1016/j.energy.2017.11.095

Niu, Q., Pan, J., Cao, L., Ji, Z., Wang, H., Wang, K., et al. (2017b). The evolution and formation mechanisms of closed pores in coal. *Fuel* 200, 555–563. doi:10.1016/j.fuel.2017.03.084

Niu, Q., Pan, J., Jin, Y., Wang, H., Li, M., Ji, Z., et al. (2019b). Fractal study of adsorption-pores in pulverized coals with various metamorphism degrees using N_2 adsorption, X-ray scattering and image analysis methods. *J. Petroleum Sci. Eng.* 176, 584–593. doi:10.1016/j.petrol.2019.01.107

Niu, Q., Wang, Q., Wang, W., Chang, J., Chen, M., Wang, H., et al. (2022). Responses of multi-scale microstructures, physical-mechanical and hydraulic characteristics of roof rocks caused by the supercritical CO_2-water-rock reaction. *Energy* 238, 121727. doi:10.1016/j.energy.2021.121727

Niu, Q., Wang, W., Liang, J., Yuan, W., Wen, L., Chang, J., et al. (2020b). Investigation of the CO_2 flooding behavior and its collaborative controlling factors. *Energy fuels.* 34, 11194–11209. doi:10.1021/acs.energyfuels.0c01286

Pan, J., Niu, Q., Wang, K., Shi, X., and Li, M. (2016). The closed pores of tectonically deformed coal studied by small-angle X-ray scattering and liquid nitrogen adsorption. *Microporous Mesoporous Mater.* 224, 245–252. doi:10.1016/j.micromeso.2015.11.057

Pan, Z., and Connell, L. D. (2011). Modelling of anisotropic coal swelling and its impact on permeability behaviour for primary and enhanced coalbed methane recovery. *Int. J. Coal Geol.* 85, 257–267. doi:10.1016/j.coal.2010.12.003

Pan, Z., Ye, J., Zhou, F., Tan, Y., Connell, L. D., and Fan, J. (2018). CO_2 storage in coal to enhance coalbed methane recovery: A review of field experiments in China. *Int. Geol. Rev.* 60, 754–776. doi:10.1080/00206814.2017.1373607

Peng, Y., Liu, J., Pan, Z., Connell, L. D., Chen, Z., and Qu, H. (2017). Impact of coal matrix strains on the evolution of permeability. *Fuel* 189, 270–283. doi:10.1016/j.fuel.2016.10.086

Rao, A. B., and Rubin, E. S. (2002). A technical, economic, and environmental assessment of amine-based CO_2 capture technology for power plant greenhouse gas control. *Environ. Sci. Technol.* 36, 4467–4475. doi:10.1021/es0158861

Rodrigues, C. F., Laiginhas, C., Fernandes, M., Lemos De Sousa, M. J., and Dinis, M. A. P. (2014). The coal cleat system: A new approach to its study. *J. Rock Mech. Geotechnical Eng.* 6, 208–218. doi:10.1016/j.jrmge.2014.03.005

Shi, J., Durucan, S., and Fujioka, M. (2008). A reservoir simulation study of CO_2 injection and N_2 flooding at the Ishikari coalfield CO_2 storage pilot project. *Jpn. Int. J. Greenh. Gas. Con.* 2, 47–57. doi:10.1016/s1750-5836(07)00112-0

Shi, X., Pan, J., Hou, Q., Jin, Y., Wang, Z., Niu, Q., et al. (2018). Micrometer-scale fractures in coal related to coal rank based on micro-CT scanning and fractal theory. *Fuel* 212, 162–172. doi:10.1016/j.fuel.2017.09.115

Shi, Y., Jia, Y., Pan, W., Huang, L., Yan, J., and Zheng, R. (2017). Potential evaluation on CO_2-EGR in tight and low-permeability reservoirs. *Nat. Gas. Ind. B* 4, 311–318. doi:10.1016/j.ngib.2017.08.013

van Bergen, F., Pagnier, H., and Krzystolik, P. (2006). Field experiment of enhanced coalbed methane-CO_2 in the upper Silesian basin of Poland. *Environ. Geosci.* 13, 201–224. doi:10.1306/eg.02130605018

Wang, J. G., Liu, J., and Kabir, A. (2013). Combined effects of directional compaction, non-Darcy flow and anisotropic swelling on coal seam gas extraction. *Int. J. Coal Geol.* 109-110, 1–14. doi:10.1016/j.coal.2013.01.009

Wang, R., Wang, Q., Niu, Q., Pan, J., Wang, H., and Wang, Z. (2020). CO_2 adsorption and swelling of coal under constrained conditions and their stage-change relationship. *J. Nat. Gas Sci. Eng.* 76, 103205. doi:10.1016/j.jngse.2020.103205

Wang, Z., Fu, X., Hao, M., Li, G., Pan, J., Niu, Q., et al. (2021). Experimental insights into the adsorption-desorption of CH_4/N_2 and induced strain for medium-rank coals. *J. Petroleum Sci. Eng.* 204, 108705. doi:10.1016/j.petrol.2021.108705

Wang, Z., Fu, X., Pan, J., Niu, Q., Zhou, H., and Zhai, Y. (2019). The fracture anisotropic evolution of different ranking coals in Shanxi Province, China. *J. Petroleum Sci. Eng.* 182, 106281. doi:10.1016/j.petrol.2019.106281

Wang, Z., Pan, J., Hou, Q., Niu, Q., Tian, J., Wang, H., et al. (2018a). Changes in the anisotropic permeability of low-rank coal under varying effective stress in Fukang mining area, China. *Fuel* 234, 1481–1497. doi:10.1016/j.fuel.2018.08.013

Wang, Z., Pan, J., Hou, Q., Yu, B., Li, M., and Niu, Q. (2018b). Anisotropic characteristics of low-rank coal fractures in the Fukang mining area, China. *Fuel* 211, 182–193. doi:10.1016/j.fuel.2017.09.067

Wei, Q., Li, X., Hu, B., Zhang, X., Zhang, J., He, Y., et al. (2019). Reservoir characteristics and coalbed methane resource evaluation of deep-buried coals: A case study of the No.13–1 coal seam from the panji deep area in huainan coalfield, southern north China. *J. Petroleum Sci. Eng.* 179, 867–884. doi:10.1016/j.petrol.2019.04.100

Wen, H., Cheng, X., Chen, J., Zhang, C., Yu, Z., Li, Z., et al. (2020). Micro-pilot test for optimized pre-extraction boreholes and enhanced coalbed methane recovery by injection of liquid carbon dioxide in the Sangshuping coal mine. *Process Saf. Environ. Prot.* 136, 39–48. doi:10.1016/j.psep.2019.12.036

Xie, H. P., Wu, L. X., and Zheng, D. Z. (2019). Prediction on the energy consumption and coal demand of China in 2025. *J. China Coal Soc.* 44 (7), 1949–1960. doi:10.13225/j.cnki.jccs.2019.0585

Xu, L., Li, Q., Myers, M., Chen, Q., and Li, X. (2019). Application of nuclear magnetic resonance technology to carbon capture, utilization and storage: A review. *J. Rock Mech. Geotechnical Eng.* 11, 892–908. doi:10.1016/j.jrmge.2019.01.003

Zhang, G., Ranjith, P. G., Liang, W., Haque, A., Perera, M. S. A., and Li, D. (2019). Stress-dependent fracture porosity and permeability of fractured coal: An *in-situ* X-ray tomography study. *Int. J. Coal Geol.* 213, 103279. doi:10.1016/j.coal.2019.103279

Zhao, Y., Zhao, G., Jiang, Y., Elsworth, D., and Huang, Y. (2014). Effects of bedding on the dynamic indirect tensile strength of coal: Laboratory experiments and numerical simulation. *Int. J. Coal Geol.* 132, 81–93. doi:10.1016/j.coal.2014.08.007

Zhou, H. W., Rong, T. L., Wang, L. J., Mou, R. Y., and Ren, W. G. (2020). A new anisotropic coal permeability model under the influence of stress, gas sorption and temperature: Development and verification. *Int. J. Rock Mech. Min. Sci.* 132, 104407. doi:10.1016/j.ijrmms.2020.104407